# Synthesis of Silver Nanoparticles Based on Hydrophobic Interface Regulation and Its Application of Electrochemical Catalysis

Wushuang Bai,[†] Qinglin Sheng,[†] Xiaoyan Ma,[‡] and Jianbin Zheng*[,†]

[†]Institute of Analytical Science, Shaanxi Provincial Key Laboratory of Electroanalytical Chemistry, Northwest University, Xi'an, Shaanxi 710069, China

[‡]The Department of Applied Chemistry, School of Sciences, Northwestern Polytechnical University, Xi'an, Shaanxi 710072, China

S *Supporting Information*

ABSTRACT: It has been shown that the aggregation of particles is a big challenge in synthetics progress due to the Brownian movement and van der Waals potential among the particles. Thus, how to avoid aggregation to synthesize nanoparticles with homogeneous morphology has been greatly impressed by considerable researchers and many strategies have been implemented to solve the problem in recent years. In this paper, a novel method for silver nanoparticles (AgNPs) synthesize based on the regulation of hydrophobic interface was proposed, studies showed that in the presence of hydrophobic polyhedral oligomeric silsesquioxane (POSS), AgNPs with homogeneous morphology grown on interface between GO and silver nitrate ($AgNO_3$) solution through a kind of common chemical reduction, and aggregation of AgNPs is avoided effectively without any protection under room temperature. The possible mechanism is discussed and the obtained AgNPs−POSS/rGO nanocomposites are used to fabricate electrochemical sensor for nitrobenzene, *p*-nitroaniline, and *p*-nitrobenzoic acid sensing. The composites have good ability to catalyze nitroaromatic compounds with the broad linear ranges of 0.5−155 ppm, 0.1−77 ppm, and 0.05−330 ppm and the low detection limits of 0.1, 0.05, and 0.02 ppm, respectively. The novel method provides a new platform for the synthesis of nanomaterials, the idea that changing hydrophobic/hydrophilic property of substrate material for growth of namomaterial may open up the traditional synthetic minds, and it will be expected to synthesize other optical, electronic, and magnetic nanomaterials.

KEYWORDS: *Interface regulation, Silver nanoparticles, Graphene oxide, Polyhedral oligomeric silsesquioxane, Electrochemical catalysis*
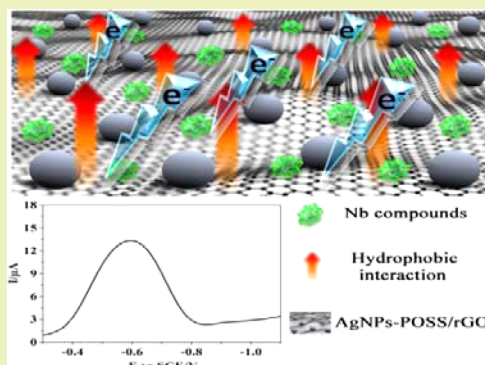
INTRODUCTION

Nowadays, nanomaterials play important roles in scientific research due to their large surface areas, high surface concentration, and other unique structure features.[1] Therefore, synthesis of nanomaterials with homogeneous morphology is a challenge for researchers. In recent decades, with the development of nanotechnology, more and more synthetic methods have been proposed and developed with integration between different disciplines, such as physical precipitation,[2] hydrothermal synthesis,[3] sol−gel,[4] template etching,[5] interfacial regulation,[6] etc. Among all the methods, interfacial regulations between different physical phases such as gas/liquid, solid/liquid, and liquid (organic phase)/liquid (aqueous phase) are so special from others, and synthesis of materials can be controlled effectively through interfacial regulation.[6−8] Hoeppener et al.[7] reported on a procedure that leads to the formation of linearly arranged ligand stabilized Au_{55} clusters, this approach utilized the incorporation of chemically modified Au_{55} nanoclusters into highly oriented molecular templates which was formed spontaneously at a kind of solid−liquid interface of highly oriented pyrolytic graphite. Vanmaekelbergh et al.[8] studied the self-assembly of colloidal Cd−Se/CdSAs at the

liquid/air interface, the obtained nanorods had systematic variation of length and initial concentration of dispersion. In addition, our group also designed an experimental facility based on gas/liquid interface regulation to prepare AgNPs.[6] On the basis of the silver mirror reaction, traditional glass plates were replaced by graphene oxide (GO), and the volatilized CH_2O gas was used as the reductant. The GO was dispersed into a $Ag[(NH_3)_2]^+$ solution first, and the mixture and another beaker that had CH_2O solution were put in a closed container. The $Ag[(NH_3)_2]^+$ solution can be reduced by volatilized CH_2O gas, and the modified silver mirror reaction was performed for 24 h under room temperature with continuous magnetic stirring. The system was designed on the basis of the concept of slowing down the rate of reduction and then the aggregation was avoided. From what mentioned above, nanomaterials have been synthesized by interface regulation between different phases, we call the above regulations as "macro-regulations" in the paper. However, the macro-regulations need more complex exper-

Scheme 1. Schematic Illustrations for the Formation of POSS/rGO
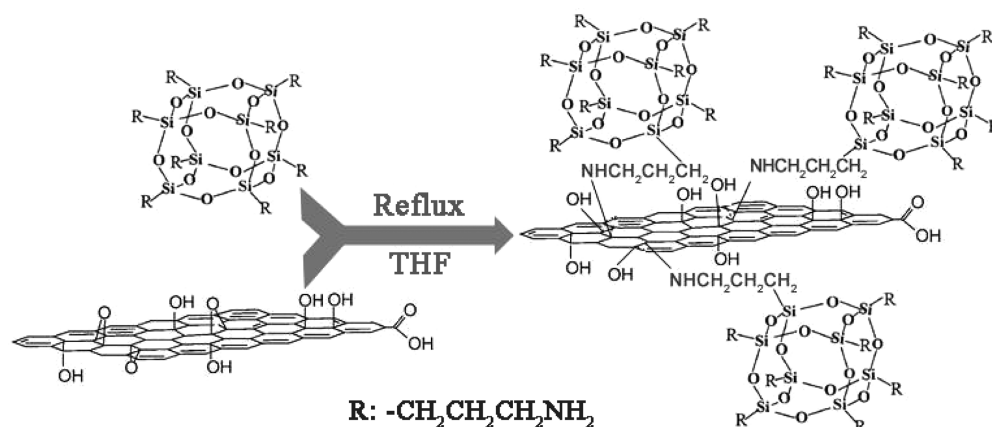
imental devices to satisfy the sufficient contact between different phases. Therefore, a novel and simple method based on a kind of so-called "micro-regulation" was proposed to synthesize AgNPs in our research.

In first step, GO was used as substrate material for growth of AgNPs. As a member of carbon materials, GO has received much attention in recent years due to its distinct physical performances (photoluminescence,[9] ferromagnetism,[10] electrodes,[11] water permeation,[12] etc.), which are derived from its unique chemical structure that composed of segregated sp^2 carbon domains among sp^3 carbons presenting various functional groups.[13] The surface of GO possesses a negative charge due to these large numbers of functional groups; therefore, it has a perfect hydrophilic property and many metal cations in a water solution can be attached on the surface.[14−20] Because of this, on the one hand, it is better for the formation of metal NPs; but on the other hand, the metal NPs are easily aggregated without any protective measures. In addition, in a previous report, aggregation of metal NPs was prevented effectively via hydrophobic interactions under harsh environmental conditions.[21] On the basis of these, in a second step, polyhedral oligomeric silsesquioxane (POSS), a kind of hydrophobic substance, was used to regulate the hydrophilic property of GO to form a hydrophobic interface for growth of AgNPs. As a kind of perfect hydrophobic substance, POSS has been used widely due to its unique cubic cage structure consisting of eight Si atoms at the corner positions bridged by oxygen along the cube edges.[22−24] After adsorption of POSS, the hydrophilic property of GO was decreased and the hydrophobic interface was formed between GO and $AgNO_3$ solution.[24] To our surprise, the aggregation was prevented successfully and the AgNPs on the surface of GO had homogeneous morphology.

In addition, because of the large surface area, good electrical conductivity, good antibacterial properties, excellent catalytic properties, and lower costs, Ag nanomaterials have been used in various fields of chemistry, physics, biology, etc.[25−28] In the field of chemistry, AgNPs are always used to fabricate electrochemical sensors to detect hydrogen peroxide, glucose, nitroaromatic, etc.,[29−32] which has attracted more interest of researchers. Golsheikh et al.[29] synthesized AgNPs-decorated graphene on indium−tin-oxide for enzymeless hydrogen peroxide detection by one-step electrodeposition; the detection limit was low and the linear range was broad. Wang et al.[30] reported a novel hydrazine sensor based on low-cost poly-

(vinylpyrrolidone)-protected silver nanocubes (PVP−AgNCs) and the sensor exhibited good reproducibility, selectivity, and stability. Roushani et al.[31] fabricated a novel, simple, and selective aptasensor for ultrasensitive detection of cocaine, the sensor was so ultrasensitive that could detect cocaine with a ultralow concentration of 150 pM. In our research, the obtained AgNPs−POSS/rGO nanocomposites were also applied to fabricate nonenzymatic electrochemical sensors to detect nitroaromatic compounds. Large surface area of GO provided more active adsorption sites for AgNPs and synergistic effect between catalysis of AgNPs and hydrophobic property of POSS may bring us more surprises in electrochemical detection.

In this paper, we report the preparation of AgNPs under hydrophobic interface regulation for the first time, and the possible mechanism of synthesis is discussed. Then obtained AgNPs−POSS/rGO nanocomposites were used for electrochemical sensing of nitroaromatic compounds. Considering the simple experiments and excellent experimental results, it is expected that the hydrophobic interface regulation may opening the new path for material synthesis and application in various fields.

■ RESULTS AND DISCUSSION

Structural and Morphological Studies. Scheme 1 shows the schematic representation for the preparation of POSS/rGO nanocomposite. The chemical bonds C−O on the surface of GO will react with the functional groups −NH₂ of POSS in the process of reflux, and POSS is attached on the surface of GO by chemical bonds C−N, the characterizations have been shown in FTIR spectra. From these, it can be seen that the combination of POSS and GO is based on chemical bonds. Therefore, the structure of POSS/rGO will be stable, and POSS will not be dropped easily from GO. However, after adsorption of POSS, hydrophilic property of GO will be decreased, the dispersion of GO will be influenced in water solution either.[24] To solve the problem, POSS/rGO nanocomposites with different mass ratios of POSS and GO were synthesized, and the dispersion in water solution was also researched, respectively. As shown in Figure S1 of the Supporting Information, pure GO can be dispersed well in water, which gives an uniform brown color (b), whereas POSS/rGO nanocomposites are difficult to be dispersed homogeneously in water with an increasing mass ratio of POSS and GO (c−f), and the solution color is changed from brown to dark gray with the increase of POSS. In addition, when the mass ratio of POSS and GO is 3:1, the

POSS/rGO nanocomposite almost cannot be dispersed in a water solution (f). As a result, the POSS/rGO nanocomposite can be dispersed in a water solution well while the mass ratio of POSS and GO is in the range from 1:2 to 2:1 (c−e).

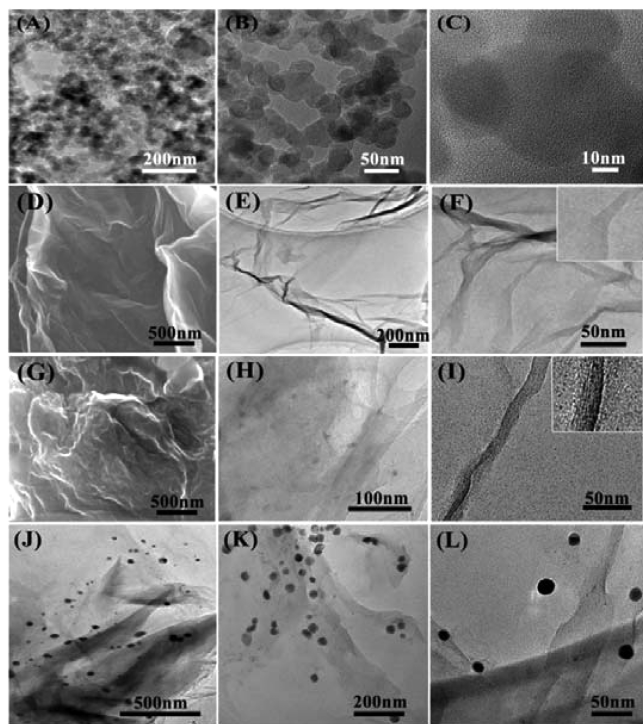Figure 1A,B,C shows the TEM patterns of POSS. As shown in patterns, POSS presents a kind of transparent and globular

Figure 1. TEM images of POSS (A, B, C), GO (E, F), POSS/rGO (H, I), AgNPs−POSS/rGO (J, K, L), and SEM images of GO (D) and POSS/rGO (G).

structure, the diameter of which is about 20 nm. Figure 1D,E,F,G,H,I shows the SEM and TEM patterns of GO and POSS/rGO, and the mass ratio of POSS and GO is 8:5. Compared with the smooth surface and monolayer structure of GO (Figure 1D,E,F), POSS/rGO has a distinctly different morphology. After adsorption of POSS, the primary smooth monolayer of GO becomes rough (Figure 1G), and it can be seen clearly that there are many dots on the surface of GO (Figure 1H,I). Figure 1J,K,L shows the TEM patterns of AgNPs−POSS/rGO nanocomposite, and the mass ratio of POSS and GO is 8:5. Although the reaction time is relatively

short, the Ag$^+$ ions are reduced quickly and the aggregation of AgNPs is avoided effectively in the presence of POSS. AgNPs are attached homogeneously on the surface of POSS/rGO (Figure 1J,K), the obtained AgNPs have uniform size, and the average diameter of particles is about 10−20 nm (Figure 1L). Meanwhile, parts of AgNPs that are not adsorbed on the surface of GO are also generated in solution, and the TEM characterizations are shown in Figure S2 of the Supporting Information. The AgNPs in solution also have relatively good morphology with a larger diameter of about 20 nm, but the dispersion of particles is not as homogeneous as the particles on the surface of GO. This may be because the hydrophobic interaction in the solution is weaker than that on the surface of GO and the aggregation is apparent to a certain extent.

The components of POSS, GO, POSS/rGO, and AgNPs− POSS/rGO have been researched, and the four samples have been characterized by FTIR, respectively (Figure 2). Figure 2A is the FTIR spectra of POSS: the peak at 3247 cm^{-1} belongs to the −NH$_2$ group and the double peaks at 2930 and 2873 cm^{-1} correspond to the C—H stretching of the CH$_2$ groups in the organic corner groups of the cage structure. The absorption band at 1103 cm^{-1} is the characteristic vibration of the Si— O—Si bond. The absorption peak at 1030 cm^{-1} is attributed to the special characteristic vibration of the silsesquioxane cage Si—O—Si framework, and the peak at 745 cm^{-1} is the bending vibration of the Si—C bond in Si—CH$_2$.[33] Figure 2B shows the FTIR spectra of (a) GO, (b) POSS/rGO, and (c) AgNPs− POSS/rGO samples. The peak at 3381 cm^{-1} is the character- istic vibration of water −OH stretching, the peaks at 1726 and 1616 cm^{-1} are attributed to C=O stretching, water −OH bending and C=C stretching, respectively. The absorption band at 1247, and 1055 cm^{-1} could be attributed to epoxide C—O—C or phenolic C—O—H stretching and C—O stretching, respectively.[34,35] Compared with GO sample, the POSS/GO shows a different absorption-peak intensity of the functional groups (b). On the basis of curve a, there are several other peaks obtained. The double peaks at 2930 and 2873 cm^{-1} in panel b correspond to the C—H stretching of the CH$_2$ groups in the organic corner groups of the unique POSS cage structure, and the absorption band at 1103 cm^{-1} is the characteristic vibration of the Si—O—Si bond, the peak at 745 cm^{-1} is the bending vibration of the Si—C bond in Si—CH$_2$, and the peak at 1355 cm^{-1} is assigned to the C—N bond. According to the FTIR spectra in panel b, POSS have been adsorbed on the surface of GO successfully. After loading of metallic Ag particles (c), the resultant composite shows a low
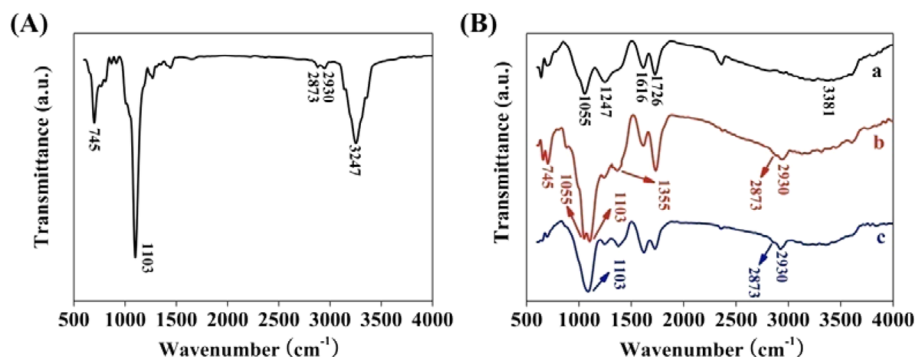

Figure 2. FTIR spectra of (A) POSS, and (B) GO (a), POSS/rGO (b), and AgNPs−POSS/rGO (c).

absorption-peak intensity of the functional groups. This may be due to the reduction effect of NaBH$_4$ on GO.

To investigate the effect of POSS on morphology of AgNPs, the AgNPs synthesized in the presence of different amount of POSS are shown in Figure 3. The mass ratios of POSS and GO
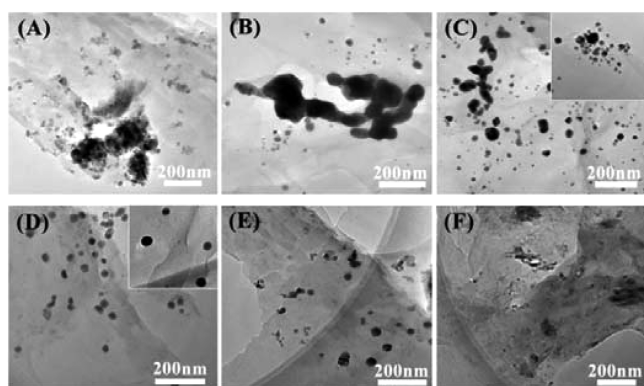

Figure 3. TEM patterns of AgNPs−POSS/rGO synthesized under different mass ratios of POSS and GO: 1:5, 3:5, 5:5, 8:5, 10:5, 13:5, respectively (from A to F).

are 1:5, 3:5, 5:5, 8:5, 10:5, 13:5, respectively (from panels A−F). As shown in Figure 3, the AgNPs are aggregated easily due to the few POSS (Figure 3A,B). When the mass ratio of POSS and GO is 5:5, it is obviously seen that the aggregation has been avoided to a certain extent (Figure 3C), and the particles are distributed more evenly on the surface of GO. However, the particles also have the trend to aggregate (inset of Figure 3C). The satisfying AgNPs can be obtained while the mass ratio of POSS and GO increases to 8:5 (Figure 3D). It is obvious that the particles have a homogeneous morphology, uniform size, and good dispersion. Meanwhile, with the increase of POSS, the adsorbed AgNPs become fewer and fewer (Figure 3E,F). When the mass ratio of POSS and GO is increased to 10:5, although obtained AgNPs still have good morphology, the amount of AgNPs on the surface of GO is decreased (Figure 3E), and there are almost no adsorbed AgNPs on the surface of GO if the mass ratio of POSS and GO becomes 13:5 (Figure 3F). From what was mentioned above, the aggregation of AgNPs is easily apparent under the condition of some POSS, it is probably due to the weaker hydrophobic interaction, and the hydrophobic interface between surface of POSS/rGO and AgNO$_3$ solution is not fully formed yet. However, when too much POSS is used, there are almost no adsorbed AgNPs on the surface of GO, probably due to the stronger hydrophobic interaction, and the POSS/rGO cannot be dispersed well in the water solution and it is difficult for the particles to attach.

In addition, the reaction temperature is also one of the main experimental factors. Figure S3 of the Supporting Information shows the TEM patterns of AgNPs−POSS/rGO nano-composites that have been synthesized under different temperatures (298, 318, and 338 K). With the increase of reaction temperature, the size of particles is increased, and parts of particles have the trend of aggregation (Figure S2B,C of the Supporting Information). So, the experimental temperature of 298 K is more appropriate for the reaction. Compared with the influence of temperature, the morphology of AgNPs changed more obviously under different addition rates of reductant (NaBH$_4$ solution, see Figure S4 of the Supporting Information). When 5 mL of a 0.1 M NaBH$_4$ solution is added at once,

the obtained AgNPs are aggregated (see Figure S3A of the Supporting Information). However, although the equal amounts of reductant are added dropwise in 30 s, the obtained AgNPs have a satisfactory morphology (see Figure S3B of the Supporting Information). When the reductant is added in 60 and 120 s, respectively, the amount and size of AgNPs decreased (see Figure S3C,D of the Supporting Information). In addition, the relationship between the morphology of AgNPs and reaction time was also studied (see Figure S5 of the Supporting Information). When the reaction time is 10 min, homogeneous AgNPs with the sizes of 10−20 nm are obtained. With the increase of reaction time, the size of AgNPs is also increased. When the reaction time is 20 min, the change of the morphology is not obvious. However, when the reaction time is 40 min, the obtained AgNPs are heterogeneous, and the size of the particles increases. In consideration of the experimental cost and the morphology of particles, the reaction time of 10 min is more appropriate.

Mechanism Analysis. Figure 4A,B shows the morphology of AgNPs that have been synthesized in the presence (A) and
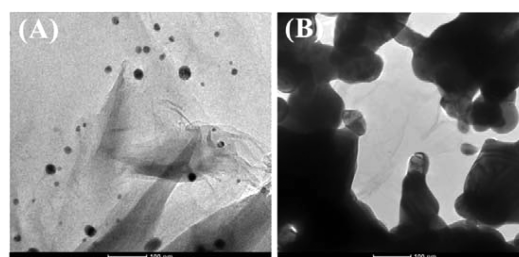

Figure 4. TEM patterns of AgNPs on the surface of GO in the presence (A) and absence (B) of POSS. The scale bars are all 100 nm.

absence (B) of POSS under the same experimental conditions. It is obviously seen that in absence of POSS, the AgNPs are seriously aggregated. The possible mechanisms are shown in Scheme 2. When GO is dispersed in AgNO$_3$ solution, because of the negative charge on the surface of GO, amounts of Ag$^+$ are attached tightly due to electrostatic adsorption, then the double layer formed (Scheme 2 A). On one hand, when large doses of reductant are added in the solution, amounts of adsorbed Ag$^+$ will be reduced soon, too many AgNPs are formed. On the one hand, under the condition of fierce chemical reaction, the movement of AgNPs is so chaotic that aggregation formed due to the Brown movement between particles and the surface of AgNPs is unprotected from van der Waals interparticle attraction, the aggregation is easily appeared (Scheme 2Ba,b).[21]

However, the situations are quite different when POSS is attached on the surface of GO. In the presence of POSS, the hydrophobic interface formed between the solution and the surface of POSS/rGO. Table 1 shows the ζ-potentials of GO, POSS/rGO, and AgNPs−POSS/rGO, respectively (the mass ratio of GO and POSS is 5:8). It can be seen obviously that the value of POSS/rGO is much higher than that of GO. According to the Gouy−Chapman pattern, the value of a ζ-potential will be decreased with the increase of concentration of bulk solution, and the double layer will become thinner. Therefore, the double layer is thicker and the local concentration of a positive ion in double layer is lower in the presence of POSS, which is due to the formation of a hydrophobic interface (Scheme 2A). When the reductant is added, on one hand,

Scheme 2. (A) Double Layer on the Surface of GO and rGO/POSS, (B) Formation of AgNPs/rGO (a, b), and AgNPs/POSS/rGO (c, d)
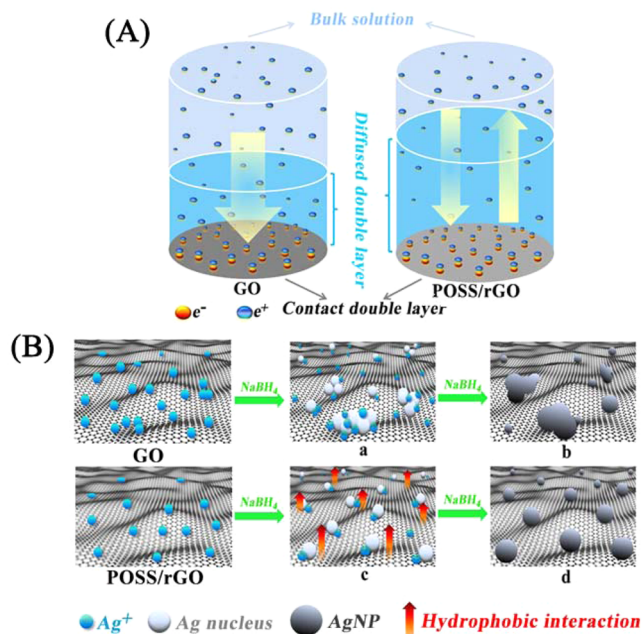
relatively fewer AgNPs are formed at first, and the Brownian movement between particles will be limited to a certain extent (Scheme 2Bc,d). On the other hand, because of the hydrophobic force of POSS/rGO, repulsion between the particles that have been attached on the surface of POSS/rGO and that are formed nearby is increased, according to the theory of DLVO, the van der Waals interparticle attraction is decreased, and then the aggregation can be avoided to a certain extent.

From what was mentioned above, in the presence of POSS, the hydrophobic interface is formed, and the aggregation of AgNPs can be avoided effectively under regulation of the hydrophobic interface.

Electrochemical Applications of AgNPs−POSS/rGO Nanocomposites. The obtained AgNPs−POSS/rGO nanocomposites have been used to fabricate electrochemical sensors. In our research, the AgNPs−POSS/rGO modified GCEs (AgNPs−POSS/rGO/GCE) have been fabricated and the obtained sensors were used for nitroaromatic compounds sensing. Electrochemical impedance spectroscopy (EIS) is an important tool to investigate the electron conduction properties of surface modified electrode. Figure 5A shows the impedance spectra of bare GCE, GO/GCE, POSS/rGO/GCE, and AgNPs−POSS/rGO/GCE. The semicircle diameter in the spectra represents electron transfer resistance (R_{ct}), and with the increase of R_{ct}, the ability of electron conduction will be decreased based on the relationship between R_{ct} and exchange current density $R_{ct} = (RT)/Fi_0$.[36] In the impedance spectra, the

value of R_{ct} is increased from 650 (a) to 950 Ω (b) after introducing POSS, which means that the resistance of POSS/rGO is higher than that of GO. However, when AgNPs are absorbed on the surface of POSS/rGO, the value of R_{ct} is decreased to 300 Ω (c), owing to the good conductivity of AgNPs. These results suggest that AgNPs could efficiently enhance the electron transfer efficiency.

To research the electrochemical changes before and after the formation of the hydrophobic interface, an unusual electrochemical measurement system has been built to measure the zero current potentials[37] of bare GCE, GO/GCE, POSS/rGO/GCE, and AgNPs−POSS/rGO/GCE. Figure 5B shows the changed three electrode system: the connectors of working electrode and counter electrode are all connected on the working electrode (bare GCE, GO/GCE, POSS/rGO/GCE, and AgNPs−rGO/POSS/GCE). When the working electrode is immersed in PBS (pH 7.2) buffer solution, an interfacial double-layer forms and the corresponding interfacial potential φ is produced. When a potential E_{app} is applied, the $I-E$ curve is recorded. In this case, the $I-E$ curve could be described by following equations:[37]

$$E_{app} = E + E_{ref} + IR + \phi \qquad (1)$$

$$I = (E_{app} - E - E_{ref} - \phi)/R \qquad (2)$$

where E_{ref} is the potential of reference electrode, I is circuit current, R is circuit resistance, and E is the potential of modified electrode held. When circuit current I is equal to zero, the potential E is named as zero current potential E_{zcp}:

$$E_{zcp} = E = E_{app} - E_{ref} - \phi \qquad (3)$$

Obviously, E_{app} and E_{ref} are constants, so the value of φ will be decreased with the E_{zcp} increasing. The results have been shown in Figure 5C, the values of E_{zcp} from large to small are (a) bare GCE, (d) AgNPs−POSS/rGO/GCE, (b) GO/GCE, and (c) POSS/rGO/GCE, respectively. Therefore, POSS/rGO/GCE has the largest interfacial potential (φ). This is probably due to the impact of the hydrophobic interface, which was discussed before.

AgNPs and GO are all common materials that are used to catalyze nitroaromatic compounds.[38] In our research, the AgNPs−POSS/rGO nanocomposites have been used for nitroaromatic compounds sensing. Figure 6A presents the differential pulse voltammetry (DPV) of GO/GCE, POSS/rGO/GCE, AgNPs−POSS/rGO/GCE, and bare GCE, (curves a, b, c, and d, respectively) in N₂-saturated 0.1 M PBS (pH 7.2). It is obviously seen that the bare GCE and modified GCEs exhibit almost no electrochemical response in the absence of NB (curves a, b, c, and d). However, after 50 ppm of NB is added, the electrochemical responses increased with varying degrees. The bare GCE shows a current peak of about 2 μA in intensity at −0.67 V (curve d′) whereas GO/GCE shows a catalytic current peak of about 5 μA in intensity at −0.7 V (curve a′). POSS/rGO/GCE shows a current response peak of about 7 μA at −0.75 V (curve b′) whereas AgNPs−POSS/

Table 1. ζ-Potential Values of GO, POSS/rGO, and AgNPs−POSS/rGO Measured Five Times, Respectively

materials	first (mV)	second (mV)	third (mV)	forth (mV)	fifth (mV)	average (mV)
GO	−34.53	−37.97	−33.00	−40.21	−39.40	−37.02
POSS/GO	−57.10	−53.66	−52.43	−59.43	−58.52	−56.23
AgNPs−POSS/GO	−56.03	−54.81	−56.99	−57.65	−57.87	−56.67

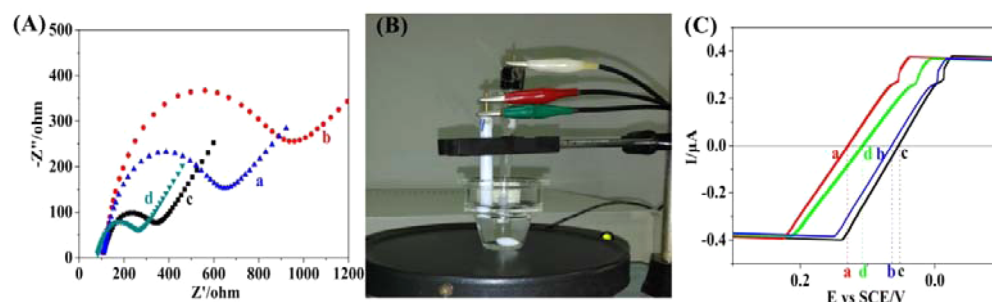**Figure 5.** (A) EIS of GO, POSS/rGO, AgNPs−POSS/rGO, and bare GCE (from a to d) in 5.0 mM $[Fe(CN)_6]^{4-/3-}$ containing 0.1 M KCl from 10^5 to 10^{-2} Hz at amplitude of 5 mV. (B) Changed three electrode system for measurement of zero current potential. (C) Zero current potentials of bare GCE, GO/GCE, POSS/rGO/GCE, and AgNPs−POSS/rGO/GCE (from a to d).
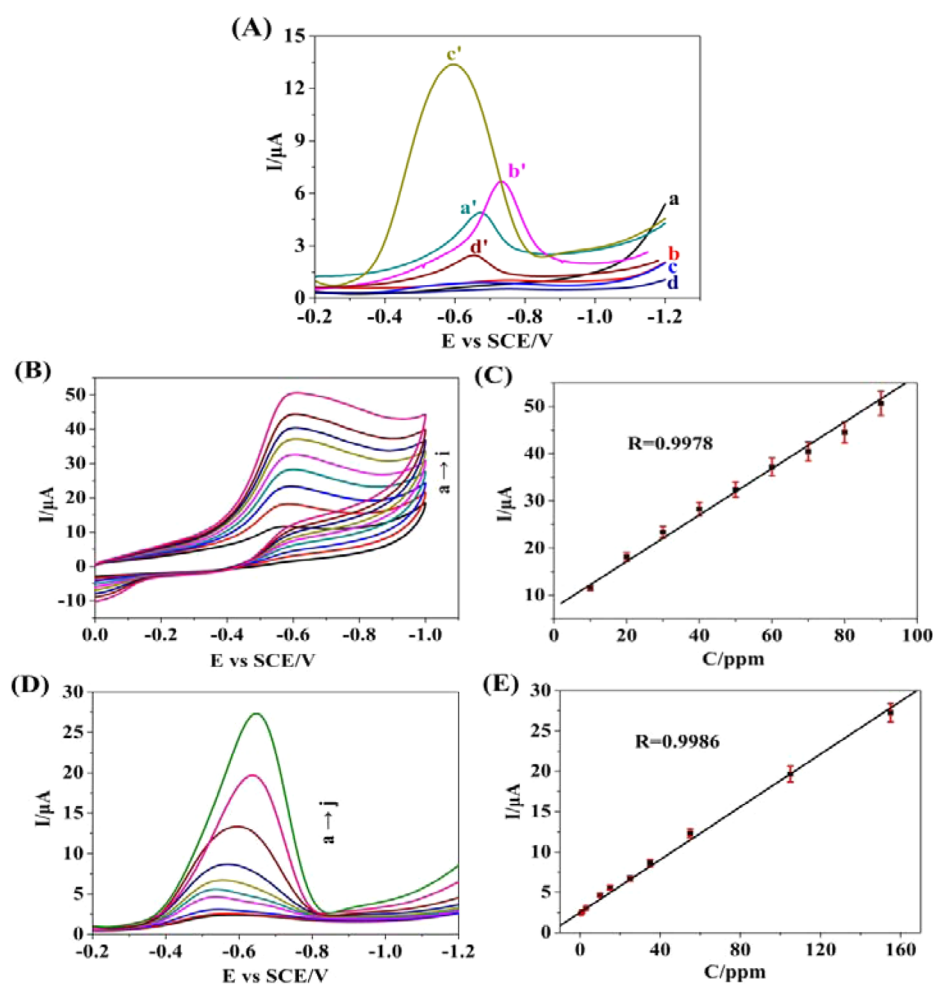

Figure 6. (A) DPVs of GO/GCE, POSS/rGO/GCE, AgNPs−POSS/rGO/GCE, and bare GCE in absence (a, b, c, and d, respectively) and presence (a′, b′, c′, and d′, respectively) of 50 ppm of NB in N_2-saturated 0.1 M PBS (pH 7.2). (B) CVs of AgNPs−POSS/rGO/GCE in N_2-saturated 0.1 M PBS (pH 7.2) in the presence of NB with different concentrations (from a to i: 10, 20, 30, 40, 50, 60, 70, 80, and 90 ppm) at a scan rate of 50 mV/s. (C) Linear fitting program of the CV reduction peak currents with the NB concentrations. (D) DPVs of AgNPs−POSS/rGO/GCE in N_2-saturated 0.1 M PBS (pH 7.2) in the presence of NB with different concentrations (from a to j: 0.5−1550 ppm). (E) Linear fitting program of the DPV reduction peak currents with the NB concentrations.

rGO/GCE shows a remarkable current peak of about 14 μA at −0.6 V (curve c′). In contrast, in the presence of POSS, the GO/GCE has a higher current response than that of bare GCE whereas the POSS/rGO/GCE has a higher current response than that of GO/GCE. This may be due to the larger surface area of POSS/GO, which has been discussed before. Although the current response of POSS/rGO/GCE is increased, the peak potential is more negative. When AgNPs are attached, the

AgNPs−POSS/rGO/GCE has the highest current response and a quite positive peak potential (curve c′). This indicates that AgNPs are a benefit for electrochemical sensing. The cyclic voltammetry (CV) curves of AgNPs−POSS/rGO/GCE, which have been obtained by changing the concentration of NB are shown in Figure 6B. It can be seen that with the increase of NB concentration (from 10 to 90 ppm), the current responses are also increased, and a good linear relationship between the
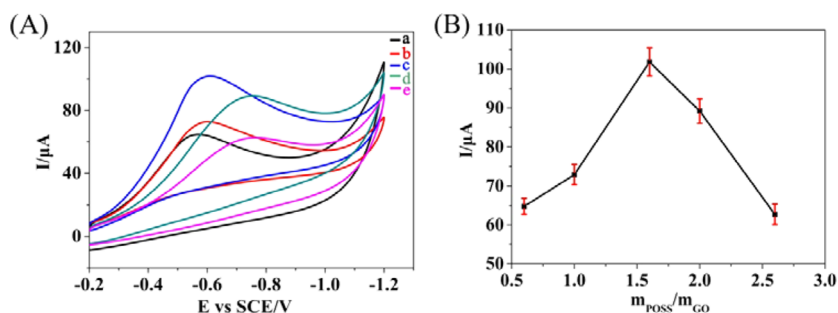
Figure 7. (A) CVs of AgNPs−POSS/rGO/GCE with different mass ratios of POSS and GO (from a to e: 3:5, 5:5, 8:5, 10:5, and 13:5, mass of GO is 5 mg) in N_2-saturated 0.1 M PBS (pH 7.2) in the presence of 200 ppm of NB. (B) Highest current response values of AgNPs−POSS/rGO/GCE with different mass ratios of POSS and GO.
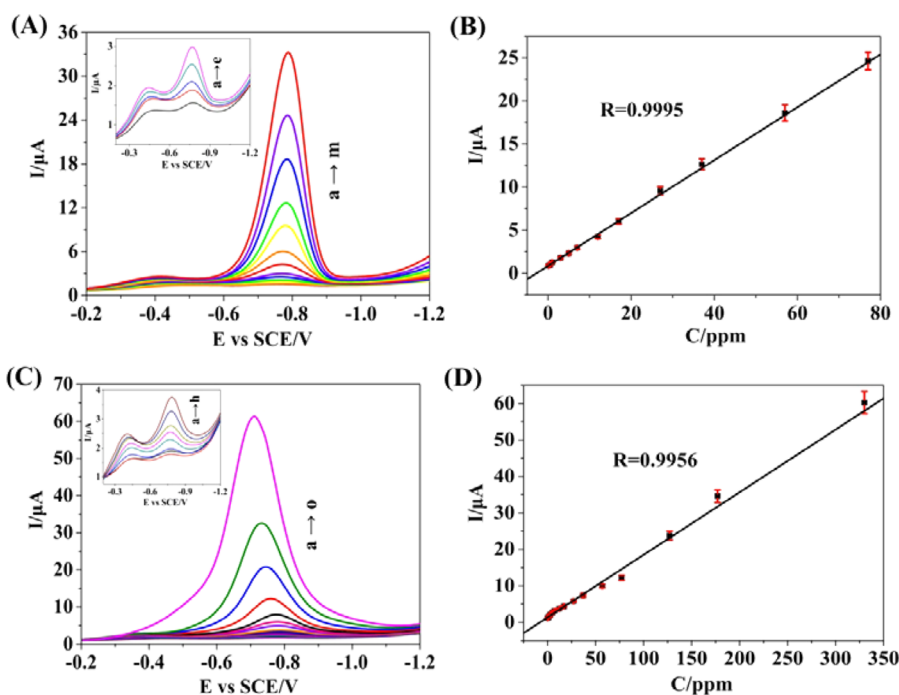

Figure 8. (A) DPVs of AgNPs−POSS/rGO/GCE in N_2-saturated 0.1 M PBS (pH 7.2) in the presence of pNA with different concentrations (from a to l: 0.1−770 ppm). (B) Linear fitting program of the reduction peak currents with the pNA concentrations. (C) DPVs of AgNPs−POSS/rGO/GCE in N_2-saturated 0.1 M PBS (pH 7.2) in the presence of pNBA with different concentrations (from a to o: 0.05−2770 ppm). (D) Linear fitting program of the reduction peak currents with the pNBA concentrations.

catalytic current and NB concentration (Figure 6C) is obtained. Figure 6D shows the DPV curves of AgNPs−POSS/rGO/GCE when different concentrations of NB are added into N_2-saturated 0.1 M PBS (pH 7.2). As shown in the DPV curves, the peak current increased with concentration. Figure 6E shows the linear relationship between the catalytic current and NB concentration, the linear detection range is 0.5−155 ppm, and the detection limit is 0.1 ppm.

To research the relationship between the concentration of POSS and current response of the sensor, the current responses of AgNPs−POSSr/GO/GCEs with different ratios of POSS and GO were explored. The current responses of AgNPs−POSS/rGO/GCEs with different mass ratios of POSS and GO are shown in Figure 7. When the mass ratio of POSS and GO is 8:5, the AgNPs−POSS/rGO/GCE has highest peak current response; however, when the amounts of POSS are too small or too large, the current responses are lower. This may be because that when the amounts of POSS are small, the obtained AgNPs have been aggregated, and when the amounts of POSS are

large, there are few AgNPs can be attached on the surface of GO (Figure 3).

In addition, AgNPs−POSS/rGO nanocomposites have been used for *p*-nitroaniline (pNA) and *p*-nitrobenzoic acid (pNBA) sensing, and the results are shown in Figure 8. We can see clearly that the composite exhibits high catalytic activity for pNA and pNBA reduction. Figure 8A,B presents the good linear relationship between reduction peak current and pNA concentration: the linear detection range is 0.1−77 ppm, and the detection limit is 0.05 ppm. Figure 8C,D shows the relationship between reduction peak current and pNBA concentration: the linear detection range is 0.05−330 ppm, and the detection limit is 0.02 ppm. Figure 9 shows the comparison of representative peak current between NB, pNA, and pNBA. With the condition of the same concentration of analyte, AgNPs−POSS/rGO/GCE exhibits the highest current response in pNA solution and the lowest current response in pNBA solution. These may attribute to the mild alkaline system (pH 7.2 N_2-saturated 0.1 M PBS). A small part of pNBA has
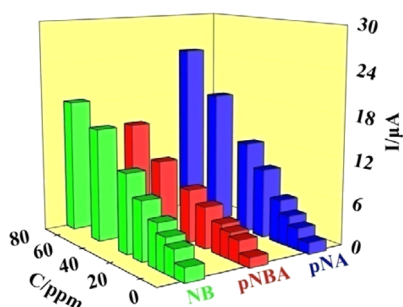
Figure 9. Representative DPV current responses of NB, pNA, and pNBA on the AgNPs−POSS/rGO/GCE at different concentrations.

been neutralized whereas pNA has the better water-solubility. Several experiments indicate that the AgNPs−POSS/rGO composite has the perfect catalytic ability for nitroaromatic compounds sensing. In addition, stability is also one of the most important properties of an electrochemical sensor. Table 2 shows the comparisons of NB peak current responses

Table 2. Comparison of NB Peak Current Responses between initial AgNPs−POSS/rGO based Sensor and That Stored in Room Environment for 1 Month (CVs of AgNPs−POSS/rGO/GCE in N_2-saturated 0.1 M PBS, 50 ppm of NB)

electrode number	initial current response (μA)	after 3 weeks (μA)
1	33.5	30.7
2	31.6	28.9
3	30.9	29.1

between initial the AgNPs−POSS/rGO based sensor and that stored in room environment for 1 month (CVs of AgNPs−POSS/rGO/GCE in N_2-saturated 0.1 M PBS). Three AgNPs−POSS/rGO/GCEs were used to detect 50 ppm, respectively. After 1 month, the modified electrodes remained more than 90% of their initial current responses. Thus, the AgNPs−POSS/rGO nanocomposites have good antioxidant ability, and AgNPs−POSS/rGO/GCE has acceptable stability. Table 3

Table 3. Comparison of the Performance of Various NB Sensors

sensors	linear range (mM)	LOD (μM)	ref
MMPCMs/GC	0.0002−0.04	0.008	40
PNMPC/GC	0.001−0.2	0.05	41
RGO−AgNPs	0.0005−0.9	0.26	42
NPC-2/GCE	0.002−0.1	0.62	43
SiO$_2$/AuNPs/GCE	0.0001−0.025	0.12	44
PEDOT/MWCNT	0.00025−0.043	0.083	45
AgNPs−POSS/rGO	0.004−1.26	0.08	this work

shows the comparison of the performance of various NB sensors. According to the comparison, it can be seen that the performance of the sensor is satisfied, the linear range is wide and the detection limit is low. In addition, the interference experiment toward O_2 has been investigated. The results are shown in Figure S6 of the Supporting Information, it can been seen that although the catalytic potential is more negative in the presence of O_2, the current response is still satisfied, which indicates that the AgNPs−POSS/rGO based sensor exhibits a good ability of anti-interference to O_2

CONCLUSION

In summary, AgNPs have been obtained without aggregation successfully in a few minutes under the regulation of a hydrophobic interface and the possible mechanisms have been analyzed. Obtained AgNPs−POSS/rGO nanocomposites have been used to fabricate electrochemical sensors for nitroaromatic compounds' sensing, and the experimental results indicate that the AgNPs−POSS/rGO nanocomposites have the perfect ability for nitroaromatic compounds catalyzing. Therefore, hydrophobic interface regulation may open a new path for materials synthesis, and the application of nanocomposites that are synthesized on the basis of hydrophobic interface regulation may promote the development of high-performance electrochemical sensors.

EXPERIMENTAL SECTION

Materials. Graphite powder (99.998%, 325 mesh, Alfa Aesar), Chitosan (CS, MW 5−6 × 10^5, >90% deacetylation) was purchased from Shanghai Yuanju Biotechnology Co., Ltd. (Shanghai, China). 0.1 M phosphate buffered saline (PBS, pH 7.2) and POSS were purchased from Hybrid Plastics (USA). All other reagents and chemicals were of analytical reagent grade, and doubly distilled water was used in experiments.

Characterization. Scanning electron microscopy (SEM) measurements were carried out on a scanning electron microscope (JSM-6700F JEOL, Japan). Transmission electron microscopy (TEM) images were carried out by a Tecnai G^2 F20 S-TWIN (FEI, USA). Fourier transform infrared spectroscopy (FTIR) was recorded with a TENSIR 27 (Bruker, Germany). ζ-Potential was measured using Zeta-PALS potential measurement analyzer (Brookhaven, USA).

Electrochemical measurements were carried out in a conventional three-electrode electroanalysis system controlled by EC 550 electrochemical workstation (Gaoss Union Technology Co., Ltd., Wuhan, China) and CHI 660 electrochemical workstation (Shanghai CH Instrument Co. Ltd., China). All electrochemical experiments were conducted at room temperature (25 ± 2 °C).

Preparation of AgNPs−POSS/rGO Nanocomposites. GO was synthesized from graphite powder.[39] Exfoliation of GO was achieved by ultrasonication of the dispersion in an ultrasonic bath.

POSS/GO was synthesized in the following steps: 5 mg of GO was dispersed into 20 mL of tetrahydrofuran containing 8 mg of POSS under sonication for 40 min. The mixture was heated to 70 °C and refluxed for 10 h under nitrogen atmosphere. Then the mixture was filtered through a 0.2 μm PTFE membrane and washed with THF three times, and then the membrane was dried in a fume cupboard at room temperature (Scheme 1).

AgNPs−POSS/rGO was synthesized by a simple method: 5 mg of POSS/rGO was dispersed in 25 mL of a water solution, and then ultrasonically mixed with 1.0 mL of 0.1 mM AgNO$_3$ solution for 30 min. Then, 5 mL 0.1 M NaBH$_4$ solutions were added in 30 s under stirring conditions, and keep reacting for 10 min. The products were separated from the solution in a centrifuge, and thoroughly washed with doubly distilled water. The obtained black powder was dried in a vacuum oven at 70 °C for 12 h.

Preparation of AgNPs−POSS/rGO Nanocomposites Modified Electrode. The glassy carbon electrode (GCE) was prepared by a simple casting method. Prior to use, the GCE was polished with 1.0 and 0.3 μm alumina powder respectively to obtain a mirror-like surface and rinsed with doubly distilled water, followed by sonication in ethanol solution and doubly distilled water successively. Then, the GCE was allowed to dry in a stream of nitrogen. The composites (1 mg) were kept in an ultrasonic dispersion for 30 min in a chitosan (1 mL, 0.5%) solution. Then the obtained suspension (5 μL) was cast onto the GCE and dried in air at room temperature. The modified electrode can be expressed as AgNPs−POSS/rGO/GCE.

ASSOCIATED CONTENT

S Supporting Information

Additional data about the TEM and electrochemical characterizations on obtained materials. The Supporting Information is available free of charge on the ACS Publications website at DOI: 10.1021/acssuschemeng.5b00297.

AUTHOR INFORMATION

Corresponding Author

*J. Zheng. E-mail: zhengjb@nwu.edu.cn. Tel./Fax: +86 29 88303448.

Notes

The authors declare no competing financial interest.

ACKNOWLEDGMENTS

REFERENCES

(1) Soreta, T. R.; Strutworf, J.; Henry, O. Electrochemical surface structuring with palladium nanoparticles for signal enhancement. *Langmuir* **2010**, *26*, 12293−12299.

(2) Zhao, Y. Y.; Fan, H. M.; Li, W. Incorporation of polyoxotungstate complexes in silica spheres and in situ formation of tungsten trioxide nanoparticles. *Langmuir* **2010**, *26*, 14894−14900.

(3) Chen, J.; Li, C.; Zhao, D. W. A quantum dot sensitized solar cell based on vertically aligned carbon nanotube templated ZnO arrays. *Electrochem. Commun.* **2010**, *12*, 1432−1435.

(4) Akpan, U. G.; Hameed, B. H. The advancements in sol−gel method of doped-TiO₂ photocatalysts. *Appl. Catal., A* **2010**, *375*, 1−11.

(5) Takahashi, Y.; Tatsuma, T. Electrodeposition of thermally stable gold and silver nanoparticle ensembles through a thin alumina nanomask. *Nanoscale* **2010**, *2*, 1494−1499.

(6) Bai, W. S.; Nie, F.; Zheng, J. B.; Sheng, Q. L. Novel silver nanoparticle−manganese oxyhydroxid−graphene oxide nanocomposite prepared by modified silver mirror reaction and its application for electrochemical sensing. *ACS Appl. Mater. Interfaces* **2014**, *6*, 5439−5449.

(7) Hoeppener, S.; Chi, L. F.; Fuchs, H. Formation of Au₅₅ strands on a molecular template at the solid−liquid interface. *Nano Lett.* **2002**, *2*, 459−463.

(8) Pietra, F.; Rabouw, F. T.; Vanmaekelbergh, D. Semiconductor nanorod self-assembly at the liquid/air interface studied by in situ GISAXS and ex situ TEM. *Nano Lett.* **2012**, *12*, 5515−5523.

(9) Loh, K. P.; Bao, Q.; Eda, G. Graphene oxide as a chemically tunable platform for optical applications. *Nat. Chem.* **2010**, *2*, 1015−1024.

(10) Wang, Y.; Huang, Y.; Song, Y. Room-temperature ferromagnetism of graphene. *Nano Lett.* **2009**, *9*, 220−224.

(11) Miller, J. R.; Outlaw, R. A.; Holloway, B. C. Graphene double-layer capacitor with ac line-filtering performance. *Science* **2010**, *329*, 1637−1639.

(12) Nair, R. R.; Wu, H. A.; Jayaram, P. N. Unimpeded permeation of water through helium-leak-tight graphene-based membranes. *Science* **2012**, *335*, 442−444.

(13) Bagri, A.; Mattevi, C.; Acik, M. Structural evolution during the reduction of chemically derived graphene oxide. *Nat. Chem.* **2010**, *2*, 581−587.

(14) Lu, L. H.; Liu, J. H.; Hu, Y. Graphene-stabilized silver nanoparticle electrochemical electrode for actuator design. *Adv. Mater.* **2013**, *25*, 1270−1274.

(15) Tang, X. Z.; Cao, Z. W.; Zhang, H. B. Growth of silver nanocrystals on graphene by simultaneous reduction of graphene oxide and silver ions with a rapid and efficient one-step approach. *Chem. Commun.* **2011**, *47*, 3084−3086.

(16) Wan, Y.; Wang, Y.; Wu, J. J. Graphene oxide sheet-mediated silver enhancement for application to electrochemical biosensors. *Anal. Chem.* **2011**, *83*, 648−653.

(17) Luo, Z. M.; Yuwen, L. H.; Han, Y. J. Reduced graphene oxide/PAMAM−silver nanoparticles nanocomposite modified electrode for direct electrochemistry of glucose oxidase and glucose sensing. *Biosens. Bioelectron.* **2012**, *36*, 179−185.

(18) He, Y.; Cui, H. Synthesis of highly chemiluminescent graphene oxide/silver nanoparticle nano-composites and their analytical applications. *J. Mater. Chem.* **2012**, *22*, 9086−9091.

(19) Si, Y. C.; Samulski, E. T. Exfoliated graphene separated by platinum nanoparticles. *Chem. Mater.* **2008**, *20*, 6792−6797.

(20) Maria, L.; Yi, C. W.; Kim, T. H. Demonstrating the capability of the high-performance plasmonic gallium graphene couple. *ACS Nano* **2014**, *8*, 3031−3041.

(21) Medina, S. D.; Blankenburg, J.; Link, S. Adsorption of a protein monolayer via hydrophobic interactions prevents nanoparticle aggregation under harsh environmental conditions. *ACS Sustainable Chem. Eng.* **2013**, *1*, 833−842.

(22) Sonia, E. L.; Maiti, A.; Jones, T. V. Polyhedral oligomeric silsesquioxane (POSS)-stabilized Pd nanoparticles: Factors governing crystallite morphology and secondary aggregate structure. *J. Phys. Chem. C* **2009**, *113*, 19424−19431.

(23) Matějka, L.; Strachota, A.; Whelan, P. Epoxy networks reinforced with polyhedral oligomeric silsesquioxanes (POSS) structure and morphology. *Macromolecules* **2004**, *37*, 9449−9456.

(24) Wang, X.; Song, L.; Yang, H. Y. Simultaneous reduction and surface functionalization of graphene oxide with POSS for reducing fire hazards in epoxy composites. *J. Mater. Chem.* **2012**, *22*, 22037−22043.

(25) Sun, Y. G.; Xia, Y. N. Shape-controlled synthesis of gold and silver nanoparticles. *Science* **2002**, *298*, 2176−2179.

(26) Lee, J. S.; Murph, W. L. Functionalizing calcium phosphate biomaterials with antibacterial silver particles. *Adv. Mater.* **2013**, *25*, 1173−1179.

(27) Kang, M. S.; Sahu, A.; Frisbie, C. D.; David, J. N. Influence of silver doping on electron transport in thin films of PbSe nanocrystals. *Adv. Mater.* **2013**, *25*, 725−731.

(28) Ayako, T.; Kazuki, N.; Norihisa, K. A localized surface plasmon resonance-based multicolor electrochromic device with electrochemically size-controlled silver nanoparticles. *Adv. Mater.* **2013**, *25*, 3197−3201.

(29) Golsheikh, A. M.; Huang, N. M.; Lim, H. N. One-step electrodeposition synthesis of silver-nanoparticle-decorated grapheme on indium-tin-oxide for enzymeless hydrogen peroxide detection. *Carbon* **2013**, *62*, 405−412.

(30) Wang, Y. H.; Yang, X. J.; Bai, J. High sensitivity hydrogen peroxide and hydrazine sensor based on silver nanocubes with rich {100} facets as an enhanced electrochemical sensing platform. *Biosens. Bioelectron.* **2013**, *43*, 180−185.

(31) Roushani, M. A novel ultrasensitive aptasensor based on silver nanoparticles measured via enhanced voltammetric response of electrochemical reduction of riboflavin as redox probe for cocaine detection. *Sens. Actuators, B* **2015**, *207*, 764−771.

(32) Song, W.; Li, H.; Liu, H. P. Fabrication of streptavidin functionalized silver nanoparticle decorated graphene and its application in disposable electrochemical sensor for immunoglobulin E. *Electrochem. Commun.* **2013**, *31*, 16−19.

(33) Valentini, L.; Bon, S. B.; Monticelli, O. Deposition of amino-functionalized polyhedral oligomeric silsesquioxanes on graphene oxide sheets immobilized onto an amino-silane modified silicon surface. *J. Mater. Chem.* **2012**, *22*, 6213−6217.

(34) Li, Q.; Guo, B. D.; Yu, J. G. Highly efficient visible-light-driven photocatalytic hydrogen production of CdS-cluster-decorated graphene nanosheets. *J. Am. Chem. Soc.* **2011**, *133*, 10878−10884.

(35) Shen, J.; Li, T.; Long, Y. One-step solid state preparation of reduced graphene oxide. *Carbon* **2012**, *50*, 2134−2140.

(36) Mano, N.; Mao, F.; Heller, A. Characteristics of a miniature compartment-less glucose-O$_2$ biofuel cell and its operation in a living plant. *J. Am. Chem. Soc.* **2003**, *125*, 6588−6594.

(37) Guo, X. X.; Song, Z. J.; Sun, J. J. Interaction of calf thymus dsDNA with anti-tumor drug tamoxifen studied by zero current potentiometry. *Biosens. Bioelectron.* **2011**, *26*, 4001−4005.

(38) Lu, X. Q.; Qi, H. T.; Zhang, X. F. Highly dispersive Ag nanoparticles on functionalized graphene for an excellent electrochemical sensor of nitroaromatic compounds. *Chem. Commun.* **2011**, *47*, 12494−12496.

(39) Luo, G. Q.; Jiang, X. J.; Li, M. Facile fabrication and enhanced photocatalytic performance of Ag/AgCl/rGO heterostructure photocatalyst. *ACS Appl. Mater. Interfaces* **2013**, *5*, 2161−2168.

(40) Ma, J. Y.; Zhang, Y. S.; Zhang, X. H. Sensitive electrochemical detection of nitrobenzene based on macro-/meso-porous carbon materials modified glassy carbon electrode. *Talanta* **2012**, *88*, 696−700.

(41) Zhang, Y. F.; Zeng, L. J.; Bo, X. J. Electrochemical study of nitrobenzene reduction using novel Pt nanoparticles/macroporous carbon hybrid nanocomposites. *Anal. Chim. Acta* **2012**, *752*, 45−52.

(42) Karuppiah, C.; Muthupandi, K.; Chen, S. M. Green synthesized silver nanoparticles decorated on reduced graphene oxide for enhanced electrochemical sensing of nitrobenzene in waste water samples. *RSC Adv.* **2015**, *5*, 31139−31146.

(43) Yan, L. J.; Bo, X. J.; Zhang, Y. F. Facile green synthesis of nitrogen-doped porous carbon and its use for electrocatalysis towards nitrobenzene and hydrazine. *Electrochim. Acta* **2014**, *137*, 693−699.

(44) Singh, S.; Devi, P.; Singh, D. Sensing behavior of silica-coated Au nanoparticles towards nitrobenzene. *Gold Bull.* **2012**, *45*, 75−81.

(45) Xu, G.; Li, B.; Wang, X. Electrochemical sensor for nitrobenzene based on carbon paste electrode modified with a poly(3,4-ethylenedioxythiophene) and carbon nanotube nanocomposite. *Microchim. Acta* **2014**, *181*, 463−469.